Available online at www.sciencedirect.com
SCIENCE DIRECT®
Journal of Computational Physics 209 (2005) 599–616
JOURNAL OF COMPUTATIONAL PHYSICS
www.elsevier.com/locate/jcp

DNS and LES of decaying isotropic turbulence with and without frame rotation using lattice Boltzmann method

Huidan Yu [a], Sharath S. Girimaji [a], Li-Shi Luo [b,*]

[a] Department of Aerospace Engineering, Texas A&M University, College Station, TX 77843-3141, USA
[b] Department of Mathematics and Statistics, Old Dominion University, Norfolk, VA 23529-0077, USA

Received 25 March 2004; received in revised form 17 March 2005; accepted 23 March 2005
Available online 23 May 2005

Abstract

The objective of the paper is to assess the effectiveness of the lattice Boltzmann equation (LBE) as a computational tool for performing direct numerical simulations (DNS) and large-eddy simulations (LES) of turbulent flows. Decaying homogeneous isotropic turbulence (HIT) in inertial and rotating frames is considered for this investigation. We perform three categories of simulations. The first category involves LBE-DNS of HIT. In the inertial frame of reference, the decay exponents of the kinetic energy k, the dissipation rate ε and the low wave-number scaling of the energy spectrum are studied. The LBE results agree well with established classical results. In the case of turbulence subject to frame rotation, the LBE simulations confirm that the energy decay rate decreases with Rossby number as the energy cascade is inhibited by rotation. Second, we carry out LBE-LES for decaying HIT in inertial frame. We compute kinetic energy decay, energy spectrum and flow structures. By comparing LBE-LES and LBE-DNS results, we observe that LBE-LES accurately captures prominent large scale flow behavior. We find that the Smagorinsky constant C_S in LBE-LES should be smaller than the typical value used in traditional Navier–Stokes (NS) LES approaches. Finally, we compare the LBE-LES and NS-LES (of comparable order of numerical accuracy) results for HIT and observe that the LBE-LES simulations appear to preserve instantaneous flow fields somewhat more accurately. Our results clearly indicate that the LBE method can accurately capture important features of decaying HIT and is potentially a reliable computational tool for turbulence simulations.

Keywords: Lattice Boltzmann equation; Decaying homogeneous isotropic turbulence in 3D; Direct numerical simulation; Large-eddy simulation; Smagorinsky model

* Corresponding author. Tel.: +1 757 683 5295; fax: +1 757 683 3885.
E-mail addresses: h0y5840@aero.tamu.edu (H. Yu), girimaji@aero.tamu.edu (S.S. Girimaji), lluo@odu.edu (L.-S. Luo).

0021-9991/$ - see front matter © 2005 Elsevier Inc. All rights reserved.
doi:10.1016/j.jcp.2005.03.022

1. Introduction

An emerging alternative to Navier–Stokes (NS) based methods for flow computations is the lattice Boltzmann method (LBM) [1–3]. The LBM is based on the Boltzmann equation and, in principle, is valid over a wider range of flow physics than the NS equations. In LBM, microscopic fluid physics is simplified to retain only the key elements (the local conservation laws and related symmetries) needed to guarantee accurate macroscopic behavior. The resulting formulation can yield computational advantages over traditional continuum methods [4–7]. Consequently, the LBM has found applications in many areas of flow physics, such as free-surface flows [8], the Rayleigh–Taylor instability between two fluids [9], multicomponent flows through porous media [10], viscoelastic flows [11,12], particulate and colloidal suspensions in fluids [13–15], and other complex systems (cf. [5–7] and refs. therein).

While LBM is reasonably well established as an efficient and effective computational tool for many flow problems, its utility in turbulence has not yet been completely investigated. In an effort to assess the ability of LBM in turbulence, we first perform direct numerical simulation (DNS) and large-eddy simulation (LES) of decaying homogeneous isotropic turbulence (HIT) in both inertial and rotating frames of reference. Decaying HIT is an important benchmark problem in DNS and LES of turbulence. In fact, the first attempt at DNS with incompressible NS equation involved this problem [16]. Since then several numerical investigations of decaying HIT have been carried out, including some recent NS studies on decay exponents and low wave-number spectra [17–20]. Some preliminary studies of three-dimensional (3D) decaying HIT using LBE have also been performed [21–23], but these investigations stop well short of quantitative comparisons with the well established classical results.

The objective of the present paper is to conduct a comprehensive numerical study of decaying HIT with LBE-DNS and LBE-LES to establish the suitability of LBM for turbulence applications. The remainder of this paper is organized as follows. Section 2 briefly reviews relevant background on decaying homogeneous isotropic turbulence. Section 3 gives a concise introduction of the lattice Boltzmann equation for DNS and LES of turbulence. Section 4 presents the numerical results and comparisons with NS-DNS and experiments. Finally, we conclude in Section 5 with a summary of our results and discussion.

As a prelude, we summarize here the simulation results and inferences. In this study, we perform the following three types of simulations. (a) LBE-DNS of decaying HIT in inertial and rotating frames of reference: the decay exponents of the kinetic energy k and dissipation rate ε are computed and compared with corresponding NS-DNS results. The low wave-number scaling of the energy spectrum is studied. The effect of rotation on the energy decay is examined. In all cases, the LBM results agree well with established data and flow behavior. (b) LBE-LES of decaying HIT in inertial frame of reference: we compute kinetic energy decay, energy spectrum and flow structures using LBE-LES. By comparing LBE-LES results with LBE-DNS, we observe that LBE-LES accurately captures large-scale flow behavior. We find that the Smagorinsky constant C_S in LBE-LES should be smaller than its traditional value used in NS-LES approaches. (c) Comparison LBE-LES vs. NS-LES: we carry out a comparative study of LBE-LES and NS-LES in HIT. Our inference is that LBE-LES preserves flow structures somewhat more accurately than NS-LES.

2. Decaying homogeneous isotropic turbulence

Decaying isotropic turbulence has been the subject of many experimental and numerical studies. Due to the vast database available, this flow is an excellent test bed for examining new numerical schemes and closure models.

The energy spectrum $\hat{E}(\boldsymbol{\kappa}, t)$ in decaying HIT evolves as

$$\partial_t \hat{E}(\boldsymbol{\kappa}, t) = -\hat{T}(\boldsymbol{\kappa}, t) - 2\nu\kappa^2 \hat{E}(\boldsymbol{\kappa}, t), \tag{1}$$

where $\boldsymbol{\kappa}$ is the wave-number and ν is the kinematic viscosity, and $\hat{T}(\boldsymbol{\kappa}, t)$ represents the nonlinear energy transfer between modes (cf. Eq. (6.162) in [24]). The kinetic energy k and dissipation rate ε are given by

$$k = \int \hat{E}(\boldsymbol{\kappa})\,\mathrm{d}\boldsymbol{\kappa}, \quad \text{and} \quad \varepsilon = 2\nu \int \kappa^2 \hat{E}(\boldsymbol{\kappa})\,\mathrm{d}\boldsymbol{\kappa}.$$

It has been long observed that, after a short initial transient period of time, the kinetic energy k and dissipation rate ε exhibit power-law decay [24]

$$\frac{k(t)}{k_0} \sim \left(\frac{t}{t_0}\right)^{-n}, \quad \frac{\varepsilon(t)}{\varepsilon_0} \sim \left(\frac{t}{t_0}\right)^{-(n+1)}, \tag{2}$$

where k_0 and ε_0 are the values of k and ε at the reference time $t_0 = n\, k_0/\varepsilon_0$ (cf. Eq. (5.277), p. 160 in [24]). Isotropic turbulence is typically characterized by the Taylor-microscale Reynolds number

$$Re_\lambda = \frac{u_{\mathrm{rms}}\lambda}{\nu} = 2k\sqrt{\frac{5}{3\nu\varepsilon}}, \tag{3}$$

where λ ($= \sqrt{15\nu u_{\mathrm{rms}}^2/\varepsilon}$) is the transverse Taylor-microscale length and u_{rms} ($= \sqrt{2k/3}$) is the root mean square (rms) of the velocity field $\boldsymbol{u}$.

Eq. (1) admits a continuous class of invariant solutions in the limit of $Re \to \infty$ [25]. At large Re, $\hat{E}(\boldsymbol{\kappa}, t)$ at the low wave-number behaves as $\lim_{\kappa\to 0}\hat{E}(\kappa) \sim \kappa^\sigma$, where σ is a time-independent constant (e.g. [26]). For inviscid fluids, if Loitsyansky's integral [27] is an invariant, then $\sigma = 4$ and $n = 10/7$ [28]; if Birkhoff's integral [29] is an invariant, then $\sigma = 2$ and $n = 6/5$ [30]. It has been recently shown that time-invariant integral length scale l corresponds to $\sigma = \infty$ and $n = 2$ and time-invariant Reynolds number corresponds to $\sigma = 1$ and $n = 1$ [31]. Furthermore, the conservation of energy, angular momentum, and helicity lead to $\sigma = 2$, 7, and 1, in the limit of $Re \to \infty$, respectively. Energy conservation in Eq. (1) leads to $\sigma = 2$, in accordance with Birkhoff's invariant [29]. Despite the apparent simplicity of the decaying HIT problem, the relevant flow invariant, asymptotic decay exponent and the low wave-number scaling are strong functions of the initial spectrum and Reynolds number. Consequently, various asymptotic behavior have been reported [17,18,25,32].

To investigate the suitability of LBE method for DNS of turbulence, we perform detailed comparisons with established data on the following important items: (i) energy decay exponent n, (ii) low wave-number scaling of the spectra, (iii) flow structure, and (iv) effect of rotation on kinetic energy decay.

3. LBE formulation for DNS and LES of turbulence

3.1. Lattice Boltzmann equation for DNS

The LBE with single-relaxation-time approximation due to Bhatnagar, Gross and Krook (BGK) [33] for the collision operator is [2,3]

$$f_\alpha(\boldsymbol{x} + \boldsymbol{e}_\alpha\delta_t, t + \delta_t) = f_\alpha(\boldsymbol{x}, t) - \frac{1}{\tau}\left[f_\alpha - f_\alpha^{(\mathrm{eq})}\right] + F_\alpha, \tag{4}$$

where f_α is the density distribution function with discrete velocity $\boldsymbol{e}_\alpha$ along the αth direction, $f_\alpha^{(\mathrm{eq})}$ is the equilibrium distribution function, and τ is the relaxation time due to fluid particle collisions. The collision time-scale determines the viscosity ν of the modeled fluid. In what follows, we use the LBE model with 19 velocities in three dimensions, i.e., the D3Q19 model. The discrete velocities are:

$$\boldsymbol{e}_\alpha = \begin{cases} (0,0) & \alpha = 0, \\ (\pm 1,0,0)c, (0,\pm 1,0)c, (0,0,\pm 1)c & \alpha = 1\text{–}6, \\ (\pm 1,\pm 1,0)c, (\pm 1,0,\pm 1)c, (\pm 1,\pm 1,0)c & \alpha = 7\text{–}18. \end{cases} \tag{5}$$

The equilibria for incompressible flow [34] are

$$f_\alpha^{(\mathrm{eq})} = w_\alpha \left\{ \delta\rho + \rho_0 \left[\frac{3\boldsymbol{e}_\alpha \cdot \boldsymbol{u}}{c^2} + \frac{9(\boldsymbol{e}_\alpha \cdot \boldsymbol{u})^2}{2c^4} - \frac{3u^2}{2c^2} \right] \right\}, \tag{6}$$

where $\delta\rho$ is the density fluctuation, ρ_0 is the constant mean density in the system which is usually set to 1, and $c = \delta_x/\delta_t = 1$ in lattice units (i.e., $\delta_t = \delta_x = 1$). The sound speed of the model is $c_s = c/\sqrt{3}$. The total density is $\rho = \rho_0 + \delta\rho$. The practice of using only $\delta\rho$ instead of ρ in Eq. (6) reduces the effect due to round-off error in the LBE simulations [35,36]. The weighting factors w_α for the D3Q19 model are $w_0 = 1/3$, $w_{1-6} = 1/18$, and $w_{7-18} = 1/36$. The mass and momentum conservations are strictly enforced by:

$$\delta\rho = \sum_\alpha f_\alpha = \sum_\alpha f_\alpha^{(\mathrm{eq})}, \quad \rho_0 \boldsymbol{u} = \sum_\alpha \boldsymbol{e}_\alpha f_\alpha = \sum_\alpha \boldsymbol{e}_\alpha f_\alpha^{(\mathrm{eq})}. \tag{7}$$

For athermal fluids, the forcing term F_α is [37]

$$F_\alpha = -3w_\alpha \rho_0 \frac{\boldsymbol{e}_\alpha \cdot \boldsymbol{a}}{c^2} \delta_t, \tag{8}$$

where $\boldsymbol{a}$ is the acceleration due to external force. In a rotating flow, $\boldsymbol{a} = -2\boldsymbol{\Omega} \times \boldsymbol{u}$ is the Coriolis force, where $\boldsymbol{\Omega}$ is the angular velocity of the frame of reference.

The Chapman–Enskog analysis of Eq. (4) leads to the following hydrodynamic equations

$$\partial_t \rho + \rho_0 \nabla \cdot \boldsymbol{u} = 0, \tag{9a}$$

$$\partial_t \boldsymbol{u} + \boldsymbol{u} \cdot \nabla \boldsymbol{u} = -\nabla p + \nu \nabla^2 \boldsymbol{u} + \boldsymbol{a}, \tag{9b}$$

where $p = c_s^2 \rho/\rho_0$, $c_s = (1/\sqrt{3})c$, and the kinematic viscosity ν has the following relation with the relaxation time

$$\nu = \frac{1}{3}\left(\tau - \frac{1}{2}\right) c^2 \delta_t. \tag{10}$$

It is important to note that in LBE the strain rate tensor S_{ij} can be obtained directly by computing the momentum fluxes Q_{ij}, which are second-order moments of the nonequilibrium distribution function:

$$\mathsf{S}_{ij} = -\frac{1}{2\rho_0 c_s^2 \tau} \mathsf{Q}_{ij}, \quad \mathsf{Q}_{ij} = \sum_\alpha e_{\alpha i} e_{\alpha j} [f_\alpha - f_\alpha^{(\mathrm{eq})}]. \tag{11}$$

The dissipation rate ε is computed as $\varepsilon = 2\nu \sum_{i,j} \mathsf{S}_{ij} \mathsf{S}_{ij}$.

3.2. LES extension of lattice Boltzmann equation

The filtered form of the LBE for LES is modeled as [38,39]:

$$\bar{f}_\alpha(\boldsymbol{x} + \boldsymbol{e}_\alpha \delta_t, t + \delta_t) = \bar{f}_\alpha(\boldsymbol{x}, t) - \frac{1}{\tau_*} [\bar{f}_\alpha - \bar{f}_\alpha^{(\mathrm{eq})}] + \bar{F}_\alpha, \tag{12}$$

where $\bar{f}_\alpha$ and $\bar{f}_\alpha^{(\mathrm{eq})}$ represent the distribution function and the equilibrium distribution function of the resolved scales, respectively. The effect of the unresolved scale motion is modeled through an effective collision relaxation time scale τ_t. Thus in Eq. (12) the total LES effective relaxation time should be $\tau_* = \tau_0 + \tau_t$,

where τ_0 and τ_t are the relaxation times corresponding to the molecular viscosity ν_0 and the turbulence or eddy viscosity ν_t, respectively. Accordingly ν_* is given by [38,39]

$$\nu_* = \nu_0 + \nu_t = \frac{1}{3}\left(\tau_* - \frac{1}{2}\right)c^2\delta_t = \frac{1}{3}\left(\tau_0 + \tau_t - \frac{1}{2}\right)c^2\delta_t, \quad \nu_t := \frac{1}{3}\tau_t c^2\delta_t, \tag{13}$$

where ν_t depends on the sub-grid model used in the simulation.

We use the Smagorinsky model [24,46] for subgrid closure. In the Smagorinsky model, the eddy viscosity ν_t is calculated from the filtered strain rate tensor $\overline{\mathsf{S}}_{ij} = (\partial_j\bar{u}_i + \partial_i\bar{u}_j)/2$ and a filter length scale Δ_x as:

$$\nu_t = (C_S\Delta_x)^2\overline{S}, \tag{14a}$$

$$\overline{S} = \frac{\overline{Q}}{2\rho_0 c_s^2\tau_*}, \quad \overline{Q} = \sqrt{2\sum_{i,j}\overline{\mathsf{Q}}_{ij}\overline{\mathsf{Q}}_{ij}}, \tag{14b}$$

where $\overline{S}$ and $\overline{Q}$ are the characteristic filtered rate of strain and the filtered mean momentum flux, respectively, and C_S is the Smagorinsky constant. Since $\tau_* = \tau_0 + \tau_t$, $\tau_0 = 3\nu_0 + 1/2$ and $\tau_t = 3\nu_t$ in lattice units, Eq. (14) leads to a quadratic equation for ν_t [39]. With C_S and Δ_x given, τ_t is obtained from Eq. (14) as

$$\tau_t = \frac{1}{2}\left(\sqrt{\tau_0^2 + 2\sqrt{2}(C_S\Delta_x)^2(\rho_0 c_s^4\delta_t)^{-1}\overline{Q}} - \tau_0\right). \tag{15}$$

In the LBE-LES with a uniform mesh, $\Delta_x = \delta_x$. In Eq. (15), the filtered momentum flux $\overline{Q}$ which is used to determine ν_t is current in time. Because the time step in the LBE simulations is relatively small in physical units, we can also use the value of $\overline{Q}$ of the previous time step to compute ν_t according to Eqs. (14), instead of Eq. (15). Furthermore, it is also possible to use finite-difference (FD) approximation for $\overline{Q}$. We will investigate all these options.

It is important to point out the salient difference between the implications of Smagorinsky closure in LBE-LES and NS-LES. In NS-LES, the subgrid stress is assumed to be in equilibrium with the instantaneous local strain. Whereas in LBE-LES, the subgrid stress is not instantly in equilibrium with filtered strain. The LBE-LES stress relaxes to the value dictated by filtered-strain at a relaxation rate determined by the current eddy-viscosity. Thus, the LBE-LES formulation may lead to more spatio-temporal memory effects. In the NS-LES, the effect of the eddy viscosity is instantaneous and the nonhydrodynamic variables are completely ignored. Some preliminary studies using the LBE-LES have yielded encouraging results [40–45]. In this work we will compare the LBE-LES and NS-LES in the fundamental problem of HIT.

In all the results presented in this paper, we use the single-relaxation-time LBE obtained from BGK model for the collision operator. Preliminary computations of LBE-DNS using a multiple-relaxation-time (MRT) model [36] show no distinguishable difference in these unforced turbulence simulations.

4. Simulation results

4.1. Initial conditions

We conduct the simulations in a 3D periodic cube with various resolutions N^3. The initial incompressible homogeneous isotropic velocity field $\boldsymbol{u}_0$ ($\nabla\cdot\boldsymbol{u}_0 = 0$) is generated in spectral space $\boldsymbol{\kappa}$ with the following energy spectrum in a prescribed range $\kappa_{\min} \leqslant \kappa \leqslant \kappa_{\max}$ and a random phase (cf. details in [47]):

$$\hat{E}(\boldsymbol{\kappa},0)=\begin{cases}0.038\kappa^m\exp(-0.14\kappa^2) & \kappa\in[\kappa_{\min},\kappa_{\max}],\\ 0 & \kappa\notin[\kappa_{\min},\kappa_{\max}].\end{cases} \tag{16}$$

Then the velocity field is transferred to physical space. In what follows, we use $m = 4$ or 2 in Eq. (16) to investigate the effect of m on the energy spectrum and other quantities.

The initial density fluctuation $\delta\rho$ (or the pressure p) consistent with the specified velocity field can be obtained by an iteration procedure [48]. It is important to stress that the preparation of the initial data is crucial in the LBE-DNS of HIT [49]. The pressure obtained by solving the Poisson equation from the initial velocity $\boldsymbol{u}_0$ is inconsistent and insufficient to initialize the LBE simulation. It is inconsistent because LBE is intrinsically compressible and, therefore, the Poisson equation is not satisfied exactly. It is insufficient because LBE initial data consists of more than the hydrodynamic variables and the nonhydrodynamic variables cannot be specified by solving hydrodynamic equations. A consistent procedure for constructing the initial data for the LBE simulation that minimizes the error due to initialization is given in [48].

4.2. LBE-DNS of decaying isotropic turbulence

We first present the results from LBE-DNS of decaying HIT in the inertial frame at two resolutions: 64^3 and 128^3. All initial spectra are given by Eq. (16) with $m = 4$ unless indicated otherwise.

Fig. 1 shows the evolutions of the normalized kinetic energy k/k_0 and the normalized dissipation rate $\varepsilon/\varepsilon_0$ with respect to normalized time $t' = t\,\varepsilon_0/k_0$. The parameters for both cases are $u_{\rm rms} = 0.023$ and $\nu = 1/600$ ($\tau = 0.505$). In the case of 64^3, the initial energy spectrum is non-zero in the range $4 \leqslant \kappa \leqslant 8$, resulting in $Re_\lambda \approx 53$. For the case of 128^3, the initial energy spectrum is non-zero in the range $1 \leqslant \kappa \leqslant 8$, resulting in $Re_\lambda \approx 119$. In the absence of production, the kinetic energy k decays monotonically in time, whereas at early stages the dissipation rate ε increases. This increase in $\varepsilon/\varepsilon_0$ is consistent with known turbulence physics (explained further below) and the same phenomenon is also seen in NS-DNS results. Following this period of increasing dissipation, both the kinetic energy and dissipation decay monotonically. The decay exponent n of the kinetic energy in these low Re_λ simulations varies in time. Furthermore, Re_λ itself is a

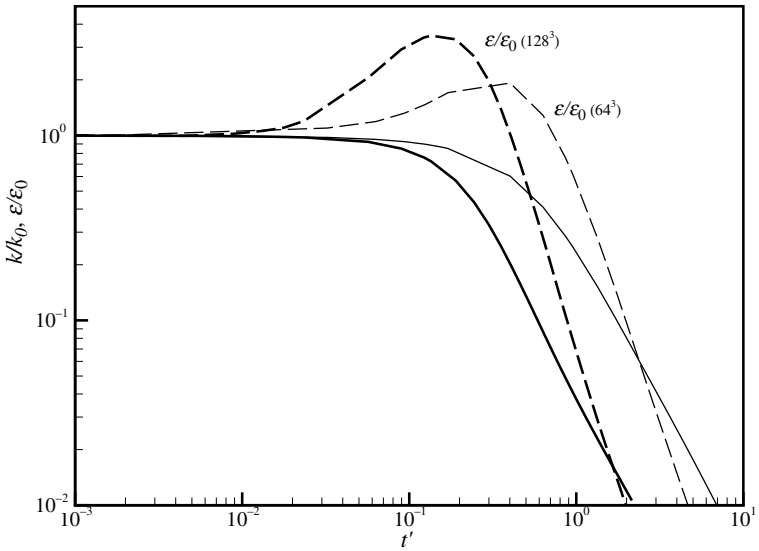

Fig. 1. Time evolution of the normalized kinetic energy k/k_0 (solid lines) and normalized dissipation rate $\varepsilon/\varepsilon_0$ (dashed lines) at two resolutions using LBE-DNS simulations. 64^3 (thin lines) and 128^3 (thick lines).

function of time as the turbulence decays. The variation of n vs. Re_λ in various simulations are shown in Fig. 2. The dependence of n on Re_λ obtained by the LBE-DNS is very similar to that observed in NS-DNS calculations [17] and experimental data.

Fig. 3(a) shows the compensated energy spectra $\hat{E}(\kappa, t')/\kappa^4$ for a 128^3 simulation at early times during which cascade is the dominant process. Initially, the spectrum (solid line; $m = 4$) is narrow and soon the energy spreads to higher wave numbers (smaller scales) due to the nonlinear cascade process. This phenomena leads to the increase of the dissipation rate in physical space, as shown in Fig. 1. This fact, in itself, is significant since advection (the source of nonlinearity) is handled very differently in LBE. At this stage, the spectrum scales as $\hat{E}(\kappa, t') \sim \kappa^4$ at small κ. Fig. 3(b) shows another 128^3 simulation which has the same rms of the initial velocity field and v as the case of Fig. 3(a), but the energy is concentrated in the range of

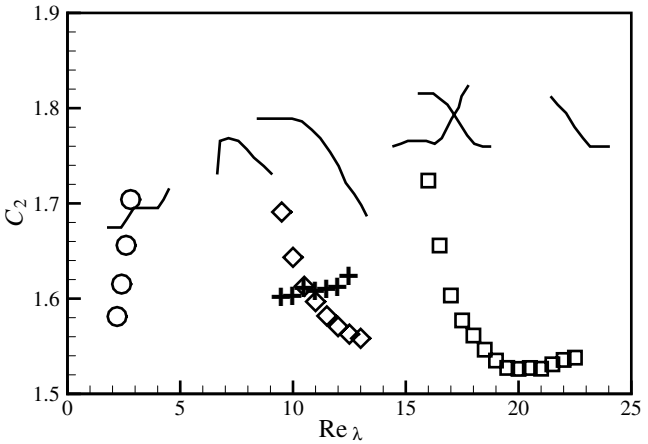

Fig. 2. Dependence of the decay exponent $n = 1/(C_2-1)$ on initial conditions and Re_λ. The quantity C_2 is depicted in the figure instead of n. Solid lines represent NS-DNS data from [17] and symbols correspond to the LBE-DNS results of the present work. For the 128^3 resolution, ○: $u_{rms} = 0.0064$, $k_{min} = 1$, $k_{max} = 8$, and $v = 0.01$; ◇: $u_{rms} = 0.021$, $k_{min} = 8$, $k_{max} = 16$, and $v = 1/600$; □: $u_{rms} = 0.022$, $k_{min} = 1$, $k_{max} = 8$, and $v = 1/600$. For the 64^3 resolution (+): $u_{rms} = 0.022$, $k_{min} = 4$ and $k_{max} = 8$, and $v = 1/600$.

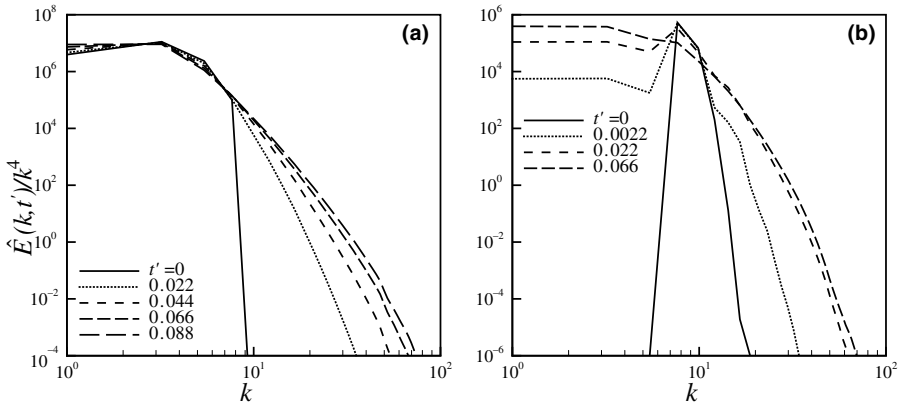

Fig. 3. Compensated energy spectra for two cases of 128^3 at early times. The initial spectra (solid lines) are given by Eq. (16) with $m = 4$. The dashed lines are the compensated energy spectra at, (a): $t' = 0.022$, 0.044, 0.066, and 0.088, and $[k_{min},k_{max}] = [1,8]$, and (b) $t' = 0.0022$, 0.022, and 0.066, and $[k_{min},k_{max}] = [8, 16]$. In both cases the spectra scale as $\hat{E}(\kappa, t') \sim \kappa^4$ at small κ.

$8 \leqslant \kappa \leqslant 16$, resulting in $Re_\lambda \approx 67$. We observe that the range $[\kappa_{\min},\kappa_{\max}]$ of the initial energy spectrum $\hat{E}(\kappa,0)$ does not affect the scaling behavior of the spectrum at later times.

Next, we show results from a set of simulations in which the initial spectrum is also given by Eq. (16) but with $m = 2$. Fig. 4 depicts the evolution of the compensated spectrum $\hat{E}(\kappa,t')/\kappa^2$ at early times. It is seen that the spectrum now scales as κ^2. In summary, as shown in Fig. 5, the low wave-number spectra scale as $\hat{E}(\kappa) \sim \kappa^4$ if $m = 4$ (Fig. 5(a)) and $\hat{E}(\kappa) \sim \kappa^2$ if $m = 2$ (Fig. 5(b)). This dependence of low-wave number scaling on initial spectrum is in agreement with the existing results (e.g. [17,18]) and theoretical predictions [50]. It can be shown by using dimensional analysis that [50], if initial spectrum is $\lim_{\kappa\to 0}\hat{E}(\kappa,0) \sim \kappa^m$ with $m \geqslant 4$, then backscatter will fill in a κ^4 spectrum at large scales (small κ). However, if $m \leqslant 4$, the low wave-number spectrum will scale as κ^m.

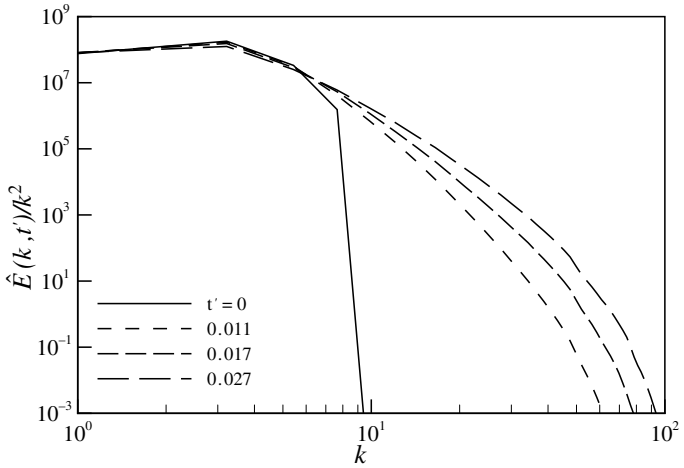

Fig. 4. Compensated energy spectra for a 128^3 simulation ($u_{\rm rms} = 0.023$, $\nu = 1/600$, and $\mathrm{Re}_\lambda \approx 141$) at early times, $t' = 0.011$, 0.017, 0.027. The initial spectra is given by Eq. (16) with $m = 2$. The spectra scale as $\hat{E}(\kappa,t') \sim \kappa^2$ at small κ.

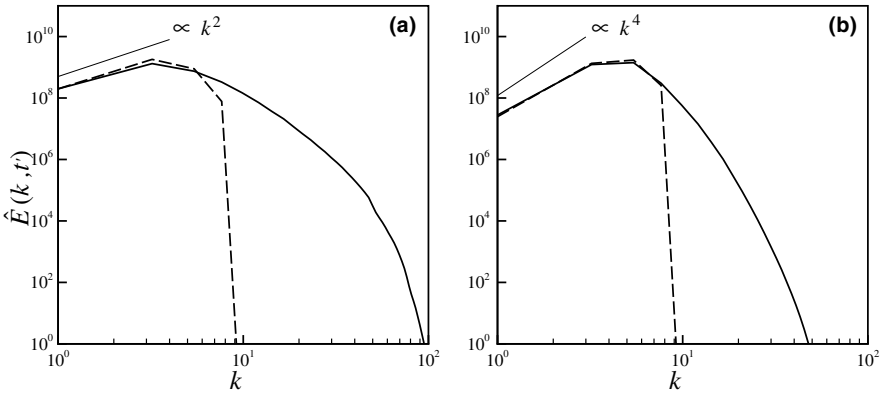

Fig. 5. Dependence of low-κ scaling on initial spectrum. The resolution is 128^3. The dash lines are initial spectra ($t' = 0$) and the solid lines are $\hat{E}(\kappa,t')$ at $t' = 0.022$. (a): $m = 2$ (corresponding to Fig. 4) and (b): $m = 4$ (corresponding to Fig. 3(a)) in Eq. (16) for the initial spectrum.

The LBE-DNS of decaying HIT in a rotating frame is also performed. Without loss of generality, we assume that the frame of reference rotates about the z-axis with the angular velocity $\mathbf{\Omega} = (0, 0, \omega)$. The Rossby number is defined as $Ro = \kappa_p u_{rms}/\omega$, where κ_p characterizes the energy containing wave number at $t = 0$. Here, we use $\kappa_p = (\kappa_{max} - \kappa_{min})/2$.

The effects of rotation are scale dependent and they are enhanced by increasing the rotation rate ω (decreasing Ro). In general, it has been well understood that rotation slows down the cascade and delays the approach to equipartition [51,52]. These features are captured in Figs. 6 and 7. Fig. 6 shows the evolution of kinetic energy at various Rossby numbers in a simulation with 128^3 resolution. The initial energy spectrum is non-zero in the range of $1 \leqslant \kappa \leqslant 8$. As expected, the energy decay slows down with decreasing Rossby number (or increasing rate of rotation). Closer examination of the spectra (Fig. 7) shows the

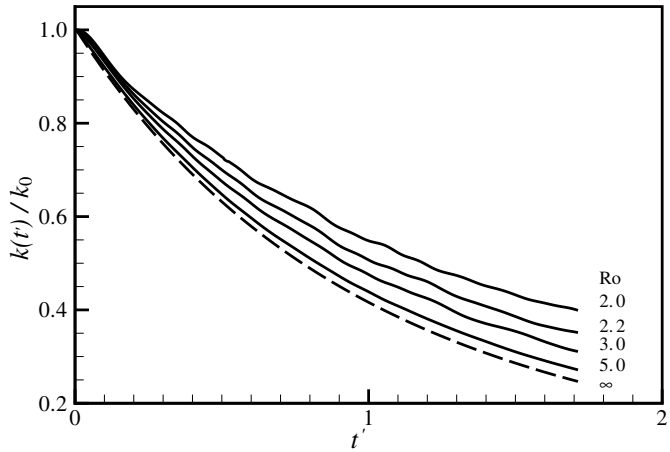

Fig. 6. Kinetic energy decay in 128^3 LBE-DNS with different Rossby (Ro) numbers.

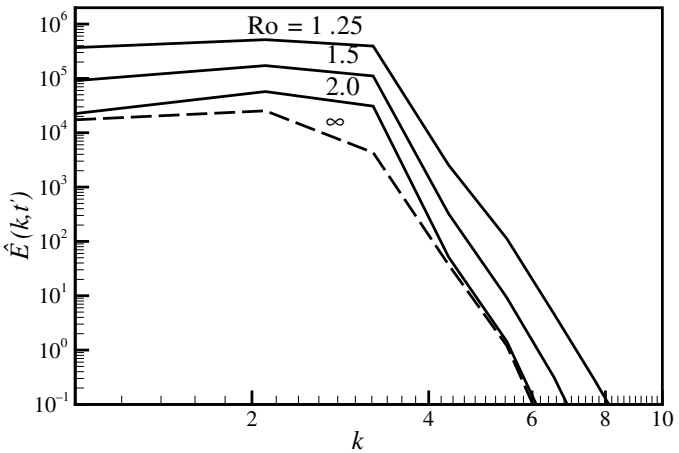

Fig. 7. Energy spectra at $t' = 10.5$ with 64^3 resolution and different Ro. $u_{rms} = 0.023$, $[k_{min}, k_{max}] = [1,4]$, and $\nu = 0.01$. The dashed line is the inertial case ($\mathbf{\Omega} = \mathbf{0}$ or $Ro = \infty$).

tendency to maintain more energy at the small wave numbers (large scales) when the system rotates. The faster the system rotates (smaller Rossby number), the more prominent is this tendency.

4.3. LBE-LES of decaying isotropic turbulence

We now turn our attention to LES with LBE. Here, we perform LES of decaying HIT without rotation. To enable close comparison with DNS, we perform LES with the initial large-scales identical to those of 128^3 LBE-DNS case (corresponding to the results of Fig. 1). The initial flow field of the LBE-DNS is appropriately truncated in spectral space to yield the initial LBE-LES fields for 32^3 and 64^3 resolutions. Thus, the initial LBE-LES field is obtained by filtering out all wave numbers above 16 for 32^3 and 32 for 64^3.

4.3.1. Calibration of C_S

Our first exercise is to determine the appropriate Smagorinsky constant for LBE-LES. Fig. 8 shows the energy spectra at some specific time instant with different Smagorinsky constant values for both 32^3 and 64^3 cases. The instantaneous LES spectra are compared against DNS spectrum at the same time. As expected, 64^3 performs better than 32^3 although at small κ (large scale) region both 32^3 and 64^3 spectra agree well with the DNS spectrum. The comparison of the kinetic energy decay from the same runs is shown in Fig. 9. From both figures, we find that $C_S = 0.1$ yields better results than the typical value of $C_S = 0.17$ used in the NS-LES [24]. The physics underlying the need for reducing C_S in LBE-LES needs further investigation.

In Fig. 10, we compare the instantaneous flow structure of $u_z(i,j,k = N/2,t')$ obtained by the LBE-LES with that calculated from LBE-DNS. As shown in Fig. 10, the LBE-LES appears to capture the flow-field structure quite adequately even with a coarse resolution of 32^3. In all subsequent calculations, we use $C_S = 0.1$.

4.3.2. Other methods of computing $\overline{S}$

In all the above calculations, we compute $\overline{S}$ from the second-order moment of nonequilibrium distribution functions at the current time-step and then determine v_t according to Eq. (15). We now investigate the other options for determining $\overline{S}$ which may provide some computational advantages.

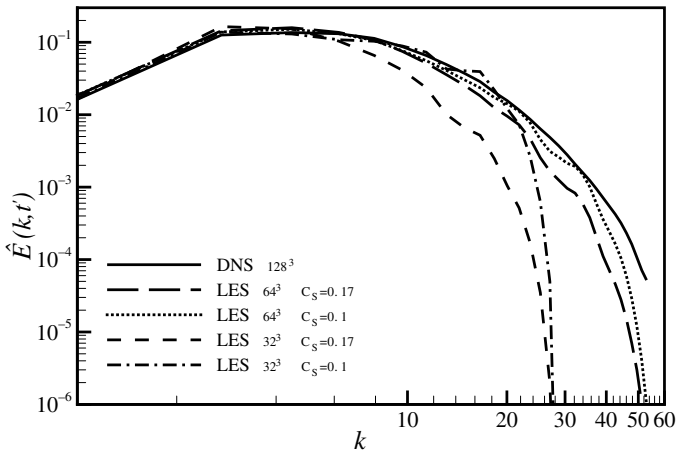

Fig. 8. Effect of C_S on the energy spectrum. The LES energy spectra at $t' = 0.04796$ with two different values of C_S (0.1 and 0.17) and two different resolutions (32^3 and 64^3) are compared with the DNS spectrum of 128^3 resolution.

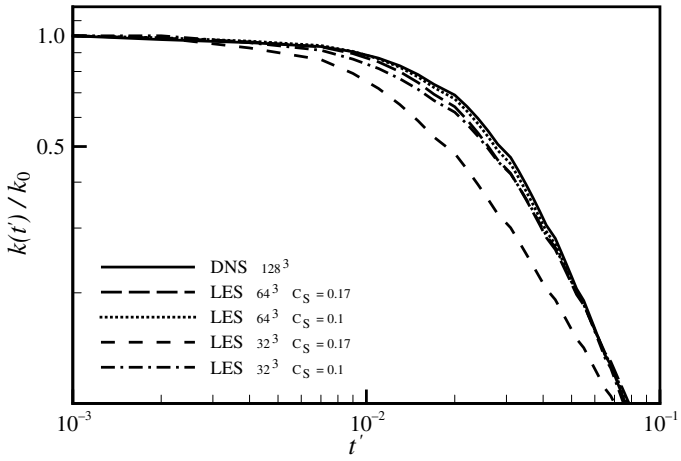

Fig. 9. Effect of C_S on the decay of the normalized kinetic energy. Same as in Fig. 8.

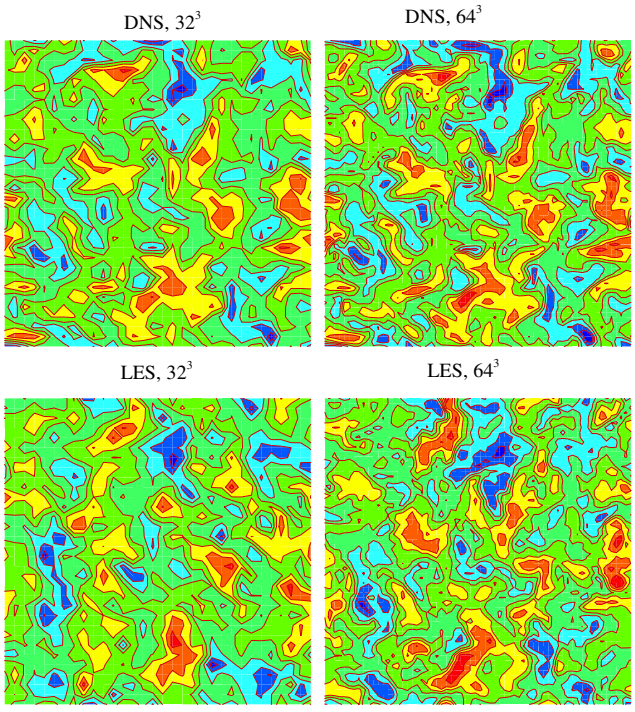

Fig. 10. Contours of the instantaneous flow field $u_z(i,j,k = N/2,t')$. LBE-DNS vs. LBE-LES with different resolutions. The 32^3 and 64^3 LBE-DNS contours shown here are obtained by truncating the 128^3 LBE-DNS data.

First, we compare two different ways of computing the strain rate tensor: (1) from the second-order moments of nonequilibrium distributions (NEQD) as given in Eq. (11) and (2) by finite-difference (FD) approximation of derivatives $\bar{S}_{ij} = (\partial_j \bar{u}_i + \partial_i \bar{u}_j)/2$. In Fig. 11, we compare the kinetic energy evolution from both computations with LBE-DNS result. In the 32^3 case (Fig. 11(a)), the computation using a simple

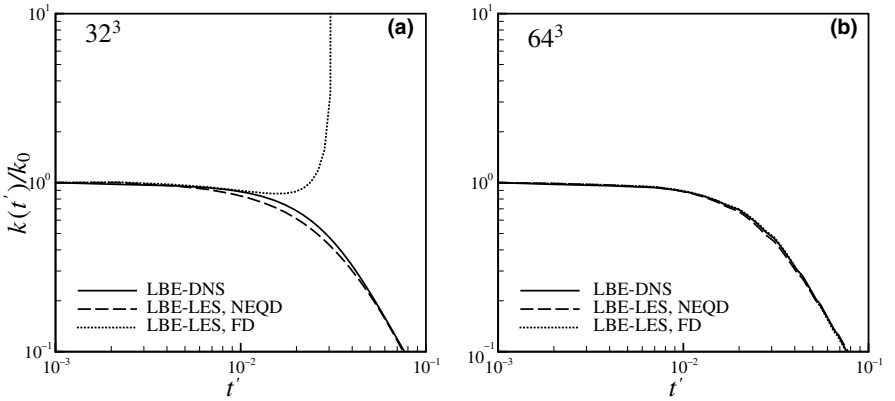

Fig. 11. Decay of kinetic energy dependence on the method of $\overline{S}_{ij}$ computation. Solid lines: LBE-DNS; dotted lines: LBE-LES, S_{ij} computed by FD; and dashed lines: LBE-LES, S_{ij} computed from NEQD. (a): 32^3 and (b): 64^3.

second-order central difference approximation quickly diverges while computation using the second-order moments of nonequilibrium distribution captures the DNS result. We also note that a more sophisticated 19-point FD approximation [53] for $\overline{\mathsf{S}}_{ij}$ does not improve the result. In the 64^3 case (Fig. 11(b)), both computations yield good results as the resolution is adequate for finite-difference evaluation of $\overline{S}$. The conclusion is that the calculation of $\overline{S}$ based on the second-order moments of the nonequilibrium distribution functions is more accurate and the corresponding LBE-LES simulations are more stable. This is more noticeable for forced turbulence flows than for decaying flows.

We next test two different methods of computing strain rate $\overline{S}$ from the second moment of nonequilibrium distribution functions. In the implicit method, v_t is computed according to Eq. (15) with $\overline{S}$ of the current time step. Whereas in the explicit approach, v_t is computed according to Eq. (14) with $\overline{S}$ from previous time step. Fig. 12 depicts the contours of the instantaneous flow structure of $u_z(i,j,k = N/2,t')$ obtained from LBE-LES (32^3) using the two formulae to compute v_t. The velocity fields obtained with the two formulae are almost identical, as shown in Fig. 12; the L^2-norm difference between the two velocity fields is less than 0.02%. Therefore, we verify that the eddy viscosity can be computed from either Eq. (15) or Eqs. (14) without significant effect on the flow fields.

4.4. LBE-LES vs. NS-LES

We further compare the LBE-LES with the NS-LES results at 32^3 resolution in Figs. 13–15. The NS solver used here is the finite-volume commercial code SWIFT [54,55], which is second-order accurate in space. A second-order NS scheme is chosen for comparison since the LBE method is formally of second order. The initial velocity fields for LBE-LES and NS-LES simulations are nearly identical. From Figs. 13 and 14, it is seen that both the normalized kinetic energy evolution $k(t')/k_0$ and the instantaneous energy spectrum $\hat{E}(\kappa, t')$ computed from LBE-LES are slightly closer to the DNS results than those computed from NS-LES.

The difference between the LBE-LES and NS-LES is much more prominent in the instantaneous flow field $u_z(i,j,k = N/2,\ t')$ as shown in Fig. 15. By comparing the LBE-LES results (left column) and the NS-LES results (right column) with the LBE-DNS results (center column), we conclude that LBE-LES preserves the flow structure marginally better than the corresponding NS-LES. The 32^3 LBE-DNS contours shown here are obtained by truncating the 128^3 LBE-DNS data.

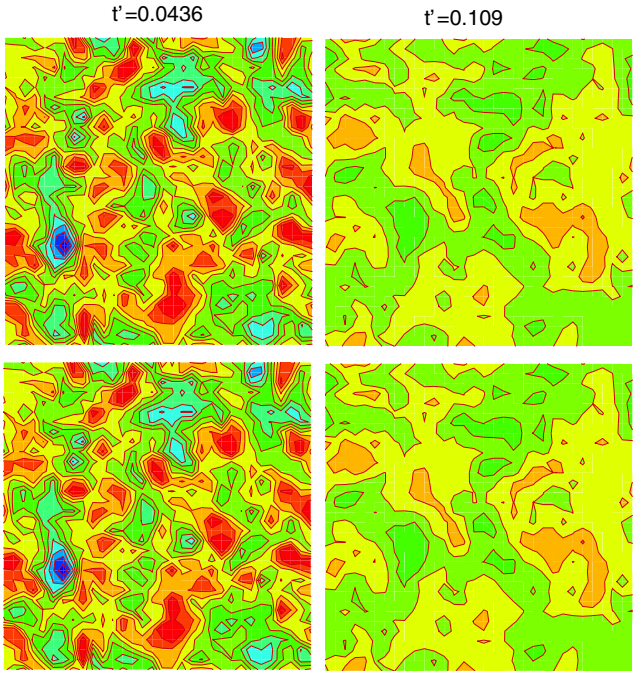

Fig. 12. The instantaneous flow field $u_z(i,j,k = N/2,t')$ obtained from LBE-LES (32^3) with two different formulae for v_t at two different times. Top row: v_t is computed according to Eq. (15). Bottom row: v_t is computed according to Eq. (14) with one-time step lag in $\overline{S}$.

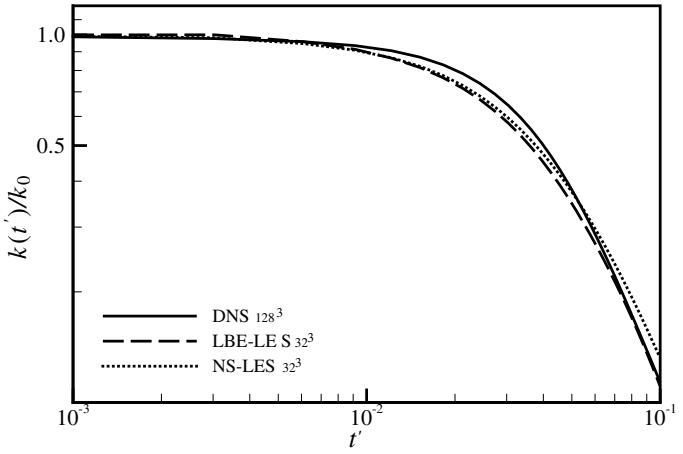

Fig. 13. Evolution of the normalized kinetic energy: LBE-LES (32^3), NS-LES (32^3), and LBE-DNS (128^3).

To quantify the difference between the LBE-LES and NS-LES, we compute the root mean squared velocity difference normalized by the total kinetic energy:

$$\Delta(\boldsymbol{u},t') = \sqrt{\frac{1}{N^3 k(t')}\sum_{i,j,k=1}^{N}[\boldsymbol{u}_{\mathrm{LES}}(i,j,k,t') - \boldsymbol{u}_{\mathrm{DNS}}(i,j,k,t')]^2}, \tag{17}$$

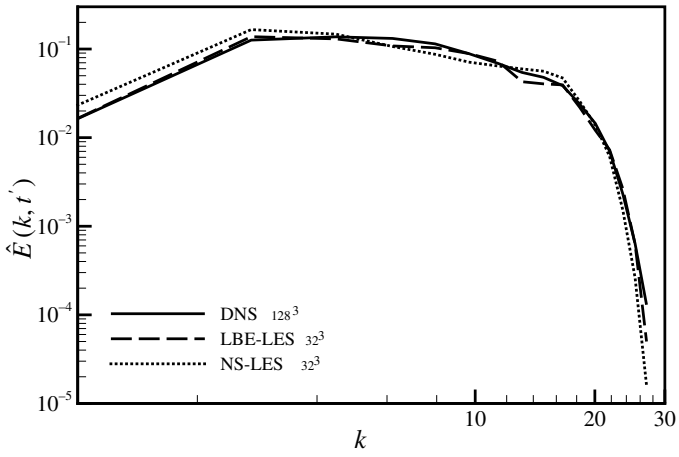

Fig. 14. The instantaneous energy spectra at $t' = 0.06079$: LBE-LES (32^3), NS-LES (32^3), and LBE-DNS (128^3).

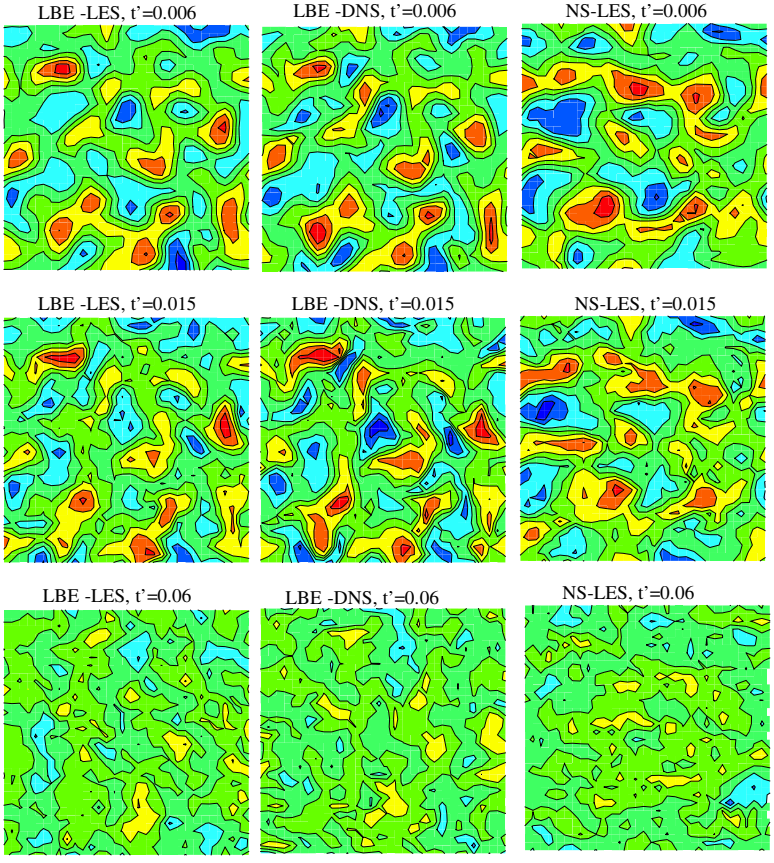

Fig. 15. The instantaneous flow field $u_z(i,j,k = N/2,t')$. The LBE-LES (32^3) and NS-LES (32^3) compared to the LBE-DNS (128^3) at three different times. The LBE-DNS data shown here is the truncated 128^3 LBE-DNS data.

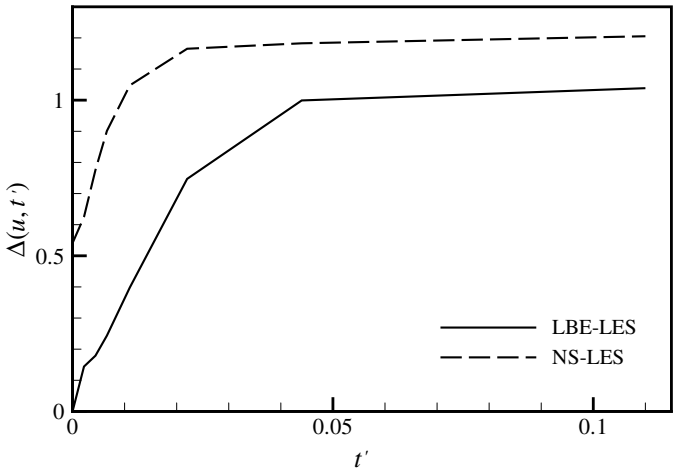

Fig. 16. Evolution of the normalized root mean squared velocity difference given by Eq. (17). LBE-LES *vs*. NS-LES, with resolution 32^3.

where $\boldsymbol{u}_{\mathrm{DNS}}$ is the 32^3 velocity field obtained from truncating the 128^3 DNS field. The errors in LBE-LES and NS-LES are shown in Fig. 16. Clearly, the LBE-LES velocity field is consistently closer to the DNS velocity field than the NS-LES counterpart. The initial incompressible velocity field $\boldsymbol{u}_0$ is generated spectrally. While the LBE-LES has no difficulty with this initial velocity field, the second-order finite-difference NS solver is incompatible with it. In the NS solver, the spectrally generated initial velocity field $\boldsymbol{u}_0$ has to be so modified that $\nabla \cdot \boldsymbol{u}_0 = 0$ is only satisfied up to second order in space. This initial difference in the velocity field persists in time, as shown in Fig. 16.

In this paper, we restrict ourselves to constant coefficient Smagorinsky subgrid closure. More recent versions of Smagorinsky model (dynamic, Lagrangian, etc.), can also be implemented on the LBE platform. There is every reason to believe that these advanced subgrid closures lead to as much improvement on the LBE platform as in the Navier–Stokes case.

The choice of the constant coefficient Smagorinsky subgrid closure for testing LBE-LES in HIT can be further justified as follows. It is well known that the deterministic value of the Smagorinsky "constant" C_{S} obtained by requiring Kolmogorov scaling of the subgrid scales and a flux balance between resolved and unresolved scales [56] is not satisfactory when used in simulations of shear flows [57]. However, it seems reasonable to expect that the dynamic procedure should return values statistically close to the deterministic value in flows in which the assumptions of Kolmogorov scaling and flux balance actually hold [58]. Both steady state forced turbulence and decaying turbulence are such flows. Indeed, simulations of homogeneous isotropic turbulence using constant C_S very close to the deterministic value are found to be satisfactory in practice [57].

5. Summary and conclusions

In this paper, we perform DNS and LES of the classical decaying HIT problem with and without reference frame rotation using the LBE method. Three categories of simulations have been performed.

First, we perform the LBE-DNS. Well known power-law decay of the kinetic energy is reproduced. The decay exponents obtained in the LBE simulations are in agreement with the results from experimental measurements and NS-DNS calculations. The low-wavenumber energy spectrum scaling depends on initial

conditions. Both κ^4 and κ^2 scaling are obtained from appropriate initial conditions consistent with [17,18]. The effect of rotation on turbulence, which is to suppress the spectral cascade, is also well captured.

Second, we conduct a comparative study of the LBE-LES and the LBE-DNS. Comparisons of 64^3 and 32^3 LBE-LES against 128^3 LBE-DNS show that the large scale motion is well captured by LBE-LES. We observe that a smaller Smagorinsky constant, $C_S = 0.1$, yields better results in LBE-LES. By choosing appropriate Smagorinsky constant C_S, even a coarse resolution of 32^3 adequately captures large scale motions.

Finally, we compare both LBE-LES and NS-LES with the corresponding DNS results and observe that LBE-LES appears to preserve instantaneous flow structure more accurately. We observe that the implications of a given subgrid closure (e.g., Smagorinsky model) can be different on the LBE platform than on an NS platform. Two major differences are now discussed. First, in LBM, the availability of nonhydrodynamic variables can potentially lead to a more accurate closure. The LBE-LES subgrid stress following a resolved streamline relaxes to the intended NS-value rather than assume the NS-value immediately. This relaxation process will clearly bring memory and non-local effects into the LBE closure that is absent in the NS platform. Second, in SGS modeling such as Smagorinsky closure, an accurate estimate of the resolved strain rate is required. The strain rate of the resolved field can be accurately calculated directly from the distribution function in LBM. In non-spectral NS methods, the strain rate has to be obtained using a finite difference procedure. The former calculation is more accurate than the latter giving LBM a potential advantage over a comparable second-order NS scheme. In fact, our results (e.g., Fig. 11(a)) show that this can make a significant difference in the calculation.

In conclusion, we would like to point out that a complete theory of the rigorous formulation of LBE-LES is still lacking. Even though our work does further validate the LBM as a viable computational tool for turbulence simulations, more extensive validation and verification studies of LBE-LES are required in the future.

Acknowledgements

H. Yu would like to thank Drs. L.-P. Wang, R. Mei, and D. Yu for helpful discussions. The authors are grateful to Dr. B. Basara for providing the NS-LES data. We are in debt to Dr. R. Rubinstein for his insightful comments regarding the ''constant'' Smagorinsky model. This work was supported by the United States Air Force Office for Scientific Research (AFOSR) under Grant No. F49620-01-1-0142.

References

[1] G.R. McNamara, G. Zanetti, Use of the Boltzmann equation to simulate lattice-gas automata, Phys. Rev. Lett. 61 (1988) 2332–2335.
[2] H. Chen, S. Chen, H.W. Matthaeus, Recovery of the Navier–Stokes equation using a lattice Boltzmann method, Phys. Rev. A 45 (1992) R5339–R5342.
[3] Y. Qian, D. d'Humières, P. Lallemand, Lattice BGK models for Navier–Stokes equations, Europhys. Lett. 17 (1992) 479–484.
[4] R. Benzi, S. Succi, M. Vergassola, The lattice Boltzmann equation: theory and applications, Phys. Rep. 222 (1992) 145–197.
[5] S. Chen, G.D. Doolen, Lattice Boltzmann method for fluid flows, Annu. Rev. Fluid Mech. 30 (1998) 329–364.
[6] L.-S. Luo, The lattice-gas and lattice Boltzmann methods: past, present and future, in: J.-H. Wu, Z.-J. Zhu, Proceedings of the International Conference on Applied CFD, October 17–20, 2000, Beijing, pp. 52–83 (Available from: <http://research.nianet.org/~luo/nonjournal-pubs.html>).
[7] D. Yu, R. Mei, L.-S. Luo, W. Shyy, Viscous flow computations with the method of lattice Boltzmann equation, Prog. Aerospace Sci. 39 (2003) 329–367.
[8] I. Ginzburg, K. Steiner, Lattice Boltzmann model for free-surface flow and its application to filling process in casting, J. Computat. Phys. 185 (2003) 61–99.

[9] T.T. Clark, A numerical study of the statistics of a two-dimensional Rayleigh–Taylor mixing layer, Phys. Fluids 15 (2003) 2413–2423.
[10] C. Pan, M. Hilpert, C. Miller, Lattice Boltzmann simulation of two-phase flow in porous media, Water Resour. Res. 40 (2004) W01501.
[11] L. Giraud, D. d'Humières, P. Lallemand, A lattice Boltzmann model for Jeffreys viscoelastic fluid, Europhys. Lett. 42 (1998) 625–630.
[12] P. Lallemand, D. d'Hmières, L.-S. Luo, R. Rubinstein, Theory of the lattice Boltzmann method: Three-dimensional model for linear viscoelastic fluids, Phys. Rev. E 67 (2003) 021203.
[13] A.J.C. Ladd, R. Verberg, Lattice-Boltzmann simulations of particle-fluid suspensions, J. Stat. Phys. 104 (2001) 1191–1251.
[14] D. Qi, L.-S. Luo, R. Aravamuthan, W. Strieder, Lateral migration and orientation of elliptical particles in Poiseuille flows, J. Stat. Phys. 107 (2002) 101–120.
[15] D. Qi, L.-S. Luo, Rotational and orientational behaviour of a three-dimensional spheroidal particles in Couette flow, J. Fluid Mech. 477 (2003) 201–213.
[16] S.A. Orszag, G.S. Patterson, Numerical simulation of three-dimensional homogeneous isotopic turbulence, Phys. Rev. Lett. 28 (1972) 76–79.
[17] N.N. Mansour, A.A. Wray, Decay of isotropic turbulence at low Reynolds number, Phys. Fluids 6 (1994) 808–814.
[18] M.-J. Huang, A. Leonard, Power-law decay of homogeneous turbulence at low Reynolds numbers, Phys. Fluids 6 (1994) 3765–3775.
[19] R. Samtaney, D.I. Pullin, B. Kosović, Direct numerical simulation of decaying compressible turbulence and shocklet statistics, Phys. Fluids 13 (2001) 1415–1430.
[20] S. Ossia, M. Lesieur, Energy backscatter in large-eddy simulations of three-dimensional incompressible isotropic turbulence, J. Turbulence 1 (2000) 010.
[21] S. Chen, Z. Wang, X. Shan, G.D. Doolen, Lattice Boltzmann computational fluid dynamics in three dimensions, J. Stat. Phys. 68 (1992) 379–400.
[22] R. Benzi, M.V. Struglia, R. Tripiccione, Extended self-similarity in numerical simulations of three-dimensional anisotropic turbulence, Phys. Rev. E 53 (1996) R5565–R5568.
[23] L.-S. Luo, L.-P. Wang, D. Qi, Applications of the lattice Boltzmann method to complex and turbulent flows, in: High Performance Scientific and Engineering Computing, in: M. Breuer, F. Durst, C. Zenger (Eds.), Lecture Notes in Computer Science and Engineering, vol. 21, Springer, Berlin, 2002, pp. 123–130.
[24] S.B. Pope, Turbulent Flows, Cambridge University Press, Cambridge, 2000.
[25] M.S. Mohamed, J.C. LaRue, The decay power law in grid-generated turbulence, J. Fluid Mech. 219 (1990) 195–214.
[26] J.C. Rotta, Turbulente Strömungen, Teubner, Stuttgart, 1972.
[27] L.G. Loitsyansky, Some basic laws for isotopic turbulent flows, Moscow Centr. Aero. Hydrodyn. Inst. Rep. No. 440, 1939 [NACA Tech. Memo. 1079 (1939)].
[28] A.N. Kolmogorov, On degeneration (decay) of isotropic turbulence in an incompressible viscous liquid, Dokl. Akad. Nauk SSSR A 31 (1941) 538–540.
[29] G. Birkhoff, Fourier synthesis of homogeneous turbulence, Comm. Pure. Appl. Math. 7 (1954) 19–44.
[30] P.G. Saffman, The large-scale structure of homogeneous turbulence, J. Fluid Mech. 27 (1967) 581–593.
[31] M. Oberlack, On the decay exponent of isotropic turbulence, Proc. Appl. Math. Mech. 1 (2002) 294–297.
[32] M.R. Smith, R.J. Donnelly, N. Goldenfeld, W.F. Vinen, Decay of vorticity in homogeneous turbulence, Phys. Rev. Lett. 71 (1993) 2583–2586.
[33] P.L. Bhatnagar, E.P. Gross, M. Krook, A model for collision processes in gases. I. Small amplitude processes in charged and neutral one-component systems, Phys. Rev. 94 (1954) 511–525.
[34] X. He, L.-S. Luo, Lattice Boltzmann model for the incompressible Navier–Stokes equation, J. Stat. Phys. 88 (1997) 927–944.
[35] P.A. Skordos, Initial and boundary conditions for the lattice Boltzmann method, Phys. Rev. E 48 (1993) 4823–4842.
[36] D. d'Humières, I. Ginzburg, M. Krafczyk, P. Lallemand, L.-S. Luo, Multiple-relaxation-time lattice Boltzmann models in three-dimensions, Philos. Trans. R. Soc. Lond. A 360 (2002) 437–451.
[37] L.-S. Luo, Theory of the lattice Boltzmann method: Lattice Boltzmann models for nonideal gases, Phys. Rev. E 62 (2000) 4982–4996.
[38] J.A. Somers, Direct simulation of fluid flow with cellular automata and the lattice-Boltzmann equation, Appl. Sci. Res. 51 (3) (1993) 127–133.
[39] S. Hou, J. Sterling, S. Chen, G.D. Doolen, A lattice Boltzmann subgrid model for high Reynolds number flows, in: Pattern Formation and Lattice Gas Automata, in: A.T. Lawniczak, R. Kapral (Eds.), Fields Inst. Comm., vol. 6, AMS, Providence, 1996, pp. 151–166.
[40] J.J. Derksen, H.E.A. Van den Akker, Large eddy simulations on the flow driven by a Rushton turbine, AIChE J. 45 (1999) 209–221.
[41] J.J. Derksen, H.E.A. Van den Akker, Simulation of vortex core precession in a reverse-flow cyclone, AIChE J. 46 (2000) 1317–1331.

[42] M. Krafczyk, Gitter-Boltzmann-Methoden: Von der Theorie zur Anwendung, Habilitation Thesis, Tech. Univ. Munich, 2001.
[43] Z. Lu, Y. Liao, D. Qian, J.B. McLauhlin, J.J. Derksen, K. Kontomaris, Large eddy simulations of a stirred tank using the lattice Boltzmann method on a nonuniform grid, J. Computat. Phys. 181 (2002) 675–704.
[44] M. Krafczyk, J. Tölke, L.-S. Luo, Large-eddy simulations with a multiple-relaxation-time LBE model, Int. J. Mod. Phys. B 17 (2003) 33–39.
[45] H. Hartmann, J.J. Derksen, C. Montavon, J. Pearson, I.S. Hamill, H.E.A. Van den Akker, Assessment of large eddy and RANS stirred tank simulations by means of LDA, Chem. Eng. Sci. 59 (2004) 2419–2432.
[46] J. Smagorinsky, General circulation experiments with the primitive equations: I. The basic equations, Mon. Weather Rev. 91 (1963) 99–164.
[47] T. Miyauchi, T. Ishizu, Direct numerical simulation of homogeneous isotropic turbulence – decay of passive scalar fluctuation, in Preprint vol. JSME No. 914-2, 1991, pp. 166–168. (Available from: <http://cfd.me.umist.ac.uk/ercofold/database/test48/test48.html>).
[48] R. Mei, L.-S. Luo, and D. d'Humières, Initial conditions for the lattice Boltzmann equation, preprint, 2001.
[49] H. Yu, S.S. Girimaji, L.-S. Luo, Lattice Boltzmann simulations of decaying homogeneous isotropic turbulence, Phys. Rev. E 91 (2005) 016708.
[50] T.T. Clark, C. Zemarch, Symmetries and the approach to statistical equilibrium in isotropic turbulence, Phys. Fluids 10 (1998) 2846–2858.
[51] Y. Yamazaki, Y. Kaneda, R. Rubinstein, Dynamics of inviscid truncated model of rotating turbulence, J. Phys. Soc. Japan 71 (2002) 81–92.
[52] J. Bardina, J.H. Ferziger, J.H. Rogallo, Effect of rotation on isotropic turbulence: Computation and modelling, J. Fluid Mech. 154 (1985) 321–336.
[53] P. Lallemand, L.-S. Luo, Theory of the lattice Boltzmann method: Acoustic and thermal properties in two and three dimensions, Phys. Rev. E 68 (2003) 036706.
[54] B. Basara, S. Jakirlic, V. Przulj, Vortex-shedding flows computed using a new, hybrid turbulence model, in: The 8th International Symposium on Flow Modeling and Turbulence Measurements (FMTM2001), December 4–6, 2001, Tokyo, Japan.
[55] B. Basara, Employment of the second-moment turbulence closure on arbitrary unstructured grids, Int. J. Numer. Meth. Fluids 44 (2004) 377–407.
[56] V. Yakhot, S.A. Orszag, Renormalization group theory of turbulence. I. Basic theory, J. Sci. Comput. 1 (1986) 3–51.
[57] K. Horiuti, A propert velocity scale for modeling subgrid-scale eddy viscosities in large eddy simulation, Phys. Fluids A 5 (1993) 146–157.
[58] R. Rubinstein, Private communication, 2005.